

Dynamics of fast neutrino flavor conversions with scattering effects: a detailed analysis

Hirokazu Sasaki^{1,*} and Tomoya Takiwaki^{2,†}

¹*Theoretical Division, Los Alamos National Laboratory, Los Alamos, New Mexico 87545, USA*

²*Division of Science, National Astronomical Observatory of Japan,
2-21-1 Osawa, Mitaka, Tokyo 181-8588, Japan*

(Dated: June 6, 2022)

We calculate fast conversions of two flavor neutrinos by considering Boltzmann collisions of neutrino scatterings. In an idealized angular distribution of neutrinos with electron-lepton number crossing, we find that the collision terms of the neutrino scattering enhance the transition probability of fast flavor conversions as in the previous study. We analyze the dynamics of fast flavor conversions with collisions in detail based on the motion of polarization vectors in cylindrical coordinate analogous to a pendulum motion. The phase of the polarization vector is partially synchronized, and the phase deviation from the Hamiltonian governs the dynamics. The collision terms break a closed orbit and gradually make the phase space smaller. The flavor conversions are enhanced during this limit cycle. After the significant flavor conversion, all of the neutrino polarization vectors start to align with the z -axis owing to the collision effect within the time scale of the collision term irrespective of neutrino scattering angles. Though our analysis does not fully understand the dynamics of fast flavor conversion, the framework gives a new insight into this complicated phenomenon in further study.

I. INTRODUCTION

There are many sources of neutrinos in our nature (see, e.g., a review in Ref. [1]). The detection of neutrinos from explosive astrophysical sites such as core-collapse supernovae (CCSNe), and neutron star mergers helps understand the mechanism of their explosive phenomena. The neutrino fluxes are affected by neutrino oscillations that are sensitive to environment inside the astrophysical sites (see, e.g., reviews in Refs. [2–4]). Coherent forward scatterings of neutrinos with background matter induce a refractive effect that has an influence on flavor conversions of neutrinos. The matter effect called the “Mikheyev-Smirnov-Wolfenstein (MSW) effect” [5, 6] is caused by charged current interactions of neutrinos with background electrons. Neutrino-neutrino interactions play important role in flavor conversions in dense neutrino gas, where large numbers of neutrinos are produced. It is numerically found that neutrino-neutrino interactions induce non-linear flavor conversions so-called “Collective neutrino oscillations” (CNOs) in CCSNe [7–22], neutron star mergers [23–31], and the early Universe [32–38]. The collective neutrino oscillations can change neutrino spectra dramatically and potentially affect neutrino signals in neutrino detectors [15, 19, 21, 22] and nucleosynthesis inside astrophysical sites such as the νp process [18, 39–41] and the r process [24, 42, 43].

Recently, much attention has been focused on fast-pair wise collective neutrino oscillations whose oscillation scales are $\sim \mathcal{O}(10^{-5})$ km (see e.g. a review [44]). The fast flavor conversions may occur near neutrino spheres and have strong impact on explosion dynamics in astrophysical sites. The possibility of fast flavor conversions

was first proposed in Ref. [45]. Fast flavor conversions are associated with anisotropic angular distribution of neutrinos [45–47]. Such fast modes are not confirmed in numerical simulations assuming the “bulb model” [7] where all of neutrinos are emitted isotropically on the surface of a fixed neutrino sphere irrespective of neutrino species and neutrino energy. The growth of instability induced by fast flavor conversions is studied through the linear stability analysis [48–51]. The instability of fast flavor conversions is studied in CCSNe [52–59] and neutron star mergers [43, 60, 61] by employing simulation data of neutrino radiation hydrodynamics. The crossing between angular distribution of ν_e and that of $\bar{\nu}_e$ so-called “electron-lepton number (ELN) crossing” is associated with fast flavor conversions [49, 62]. The methods of ELN-crossings search in multi-dimensional (multi-D) CCSNe simulations are recently developed [63–65] and such treatments are applied to state-of-the-art supernova simulations [66, 67]. In general, numerical simulations of fast flavor conversions in non-linear regime are challenging problem due to the numerical difficulties, but the fast flavor conversions can be calculated even in non-linear regime within local simulations [68–81].

The Boltzmann collision terms that correspond to contributions from incoherent scatterings, emission, and absorption of neutrinos are taken into account in simulations of collective neutrino oscillations [16, 17, 21, 70, 73, 74, 76, 79]. Neutrino scattering terms can increase the transition probability of neutrinos and neutrino spectra become anisotropic after the fast flavor conversions [73]. On the other hand, Ref. [76] shows that fast flavor conversions are damped and neutrino spectra become isotropic on the scale of the mean free path of neutrinos. These two results seem to contradict with each other and the role of Boltzmann collision on fast flavor conversions is still unknown.

In this work, we calculate fast flavor conversions in

* hsasaki@lanl.gov, [orcid: 0000-0001-9866-7003](https://orcid.org/0000-0001-9866-7003)

† takiwaki.tomoya.astro@gmail.com, [orcid: 0000-0003-0304-9283](https://orcid.org/0000-0003-0304-9283)

the non-linear regime and study the effect of neutrino scatterings on the fast flavor conversions based on the dynamics of two flavor neutrino polarization vectors. In Sec. II, we explain our numerical setup for fast flavor conversions in the non-linear regime. In Sec. III, we show the numerical results and discuss the effect of neutrino scatterings. Here, we divide the evolution of fast flavor conversions into three stages: linear evolution phase, limit cycle phase, and relaxation phase. We finally summarize our results in Sec. IV.

II. METHODS

We calculate fast flavor conversions of two flavor neutrinos (ν_e, ν_x) and antineutrinos ($\bar{\nu}_e, \bar{\nu}_x$) with collision terms of neutrino scattering based on a formalism in Ref. [73]. We analyze behaviors of the flavor conversions through the geometrical representation of neutrino density matrices. In this section, we explain numerical setup for our calculation and introduce equation of motion of polarization vectors to analyze the dynamics of flavor conversions.

Neutrino oscillations considering Boltzmann collisions are expressed by the time evolution of neutrino density matrix ρ and that of antineutrino $\bar{\rho}$ [17, 73, 76, 82–86]:

$$\frac{d}{dt}\rho = -i[H, \rho] + C[\rho, \bar{\rho}], \quad (1)$$

$$\frac{d}{dt}\bar{\rho} = -i[\bar{H}, \bar{\rho}] + \bar{C}[\rho, \bar{\rho}], \quad (2)$$

where $H(\bar{H})$ and $C(\bar{C})$ are Hamiltonian and collision term of neutrinos (antineutrinos), respectively. The time integration of the equations is performed by Runge-Kutta 4th method. We have confirmed that the results with the 5th-order method are the same as that of the 4th-order method. The time step is chosen as $\Delta t < 0.1/\max[H_{i,j,\theta}, \bar{H}_{i,j,\theta}]$, where i, j are e, x ; and the components of Hamiltonian depend on the angle, θ .

In explosive astrophysical sites without magnetic fields, neutrino Hamiltonian is composed of vacuum Hamiltonian, the MSW matter term and potential of neutrino-neutrino interactions [87]. For simplicity, the MSW matter potential is ignored in our calculation. Instead of the matter potential, we impose an effective vacuum mixing angle: $\theta_v = 10^{-6}$ that compensates the effect of matter suppression [12]. The vacuum Hamiltonian of two flavor neutrino is described by

$$H_{\text{vac}} = \frac{\omega}{2} \begin{pmatrix} -\cos 2\theta_v & \sin 2\theta_v \\ \sin 2\theta_v & \cos 2\theta_v \end{pmatrix}, \quad (3)$$

where $\omega = \frac{\Delta m^2}{2E}$ is a vacuum frequency composed of a neutrino energy E and neutrino mass difference Δm^2 . We use the small mass difference: $\Delta m^2 = 2.5 \times 10^{-6} \text{ eV}^2$ which leads to a periodic trend of fast flavor conversions [68, 71, 72]. The fast flavor conversions are associate

with angular dependence in neutrino distributions. In this work, We remove energy dependence in neutrino distribution and focus on flavor conversions of single energy neutrinos ($E = 50 \text{ MeV}$). In the case of azimuthal symmetric neutrino emission, the potential of neutrino-neutrino interaction is given by the integration over a polar angle θ [72],

$$H_{\nu\nu}(\cos \theta) = 2\pi\mu \int_{-1}^1 d\cos \theta' (1 - \cos \theta' \cos \theta) \{\rho(\cos \theta) - \bar{\rho}(\cos \theta)\}, \quad (4)$$

where μ is the strength of neutrino-neutrino interactions. Throughout the calculation, we fix the strength of neutrino-neutrino interaction as $\mu = 10^4 \text{ km}^{-1}$. To minimize the error in the integration, we employ 2000 Gauss-Legendre mesh for θ .

In general, the Boltzmann collision of neutrino scatterings should depend on neutrino energy, scattering angles and flavors. In this work, we ignore the flavor dependence in collision terms and focus on elastic scattering of neutrinos. We employ direction-changing collisions [73],

$$C[\rho, \bar{\rho}] = - \int_{-1}^1 d\cos \theta' C_{\text{loss}} \rho(\cos \theta) + \int_{-1}^1 d\cos \theta' C_{\text{gain}} \rho(\cos \theta'), \quad (5)$$

$$\bar{C}[\rho, \bar{\rho}] = - \int_{-1}^1 d\cos \theta' \bar{C}_{\text{loss}} \bar{\rho}(\cos \theta) + \int_{-1}^1 d\cos \theta' \bar{C}_{\text{gain}} \bar{\rho}(\cos \theta'), \quad (6)$$

where the first terms and second terms of the above equations represent “loss” and “gain” terms, respectively. The number of neutrinos (antineutrinos) are conserved when $C_{\text{loss}} = C_{\text{gain}}$ ($\bar{C}_{\text{loss}} = \bar{C}_{\text{gain}}$) is satisfied. Here, we assume constant collision terms: $C_{\text{loss}} = C_{\text{gain}} = \bar{C}_{\text{loss}} = \bar{C}_{\text{gain}} = C/2$ irrespective of neutrino scattering angles as followed in Refs. [73, 74].

In the beginning of the calculation ($t = 0$), we employ the distributions of ν_e and $\bar{\nu}_e$ such as

$$\begin{aligned} \rho_{ee}(\cos \theta) &= 0.5, \\ \bar{\rho}_{ee}(\cos \theta) &= 0.47 + 0.05 \exp(-2(\cos \theta - 1)^2), \end{aligned} \quad (7)$$

where ρ_{xx} and $\bar{\rho}_{xx}$ are equal to zero (see the top panel of Fig. 11). There is a ELN crossing around $\cos \theta \sim 0.5$ in Eq. (7). These initial conditions correspond to those in the Case B in Ref. [73]. We impose a random phase, i.e., $\rho_{ex} = \rho_{ee}\epsilon$, $\bar{\rho}_{ex} = \bar{\rho}_{ee}\epsilon$, where ϵ is a random complex number of the order of 10^{-8} .

In our numerical setup, the neutrino density matrix depends on the polar scattering angle θ and the time t . Hereafter, for the simple notation, we do not write the dependence explicitly. In two flavor neutrinos, the neutrino density matrix is decomposed of Pauli matrices

$\sigma_i (i = x, y, z)$ and polarization vector $\mathbf{P} = (P_x, P_y, P_z)$:

$$\rho = \begin{pmatrix} \rho_{ee} & \rho_{ex} \\ \rho_{xe} & \rho_{xx} \end{pmatrix} = \frac{\text{Tr}\rho}{2} I_{2 \times 2} + \frac{P_i \sigma_i}{2}, \quad (8)$$

where $I_{2 \times 2} = \text{diag}(1, 1)$. The density matrix of antineutrino $\bar{\rho}$ is also represented by the polarization vector of antineutrino $\bar{\mathbf{P}} = (\bar{P}_x, \bar{P}_y, \bar{P}_z)$ in the same way. In our numerical setup, the equations of motion of polarization vectors are written as

$$\begin{aligned} \frac{d}{dt} \mathbf{P} &= (+\omega \mathbf{B} + \mu' \mathbf{D}_0 - \mu' \cos \theta \mathbf{D}_1) \times \mathbf{P} - C \mathbf{P} + C \langle \mathbf{P} \rangle, \\ \frac{d}{dt} \bar{\mathbf{P}} &= (-\omega \mathbf{B} + \mu' \mathbf{D}_0 - \mu' \cos \theta \mathbf{D}_1) \times \bar{\mathbf{P}} - C \bar{\mathbf{P}} + C \langle \bar{\mathbf{P}} \rangle. \end{aligned} \quad (9)$$

The variables in the equations are defined as

$$\begin{aligned} \mathbf{B} &= (\sin 2\theta_v, 0, -\cos 2\theta_v), \\ \mathbf{D}_0 &= \langle \mathbf{P} - \bar{\mathbf{P}} \rangle, \\ \mathbf{D}_1 &= \langle (\mathbf{P} - \bar{\mathbf{P}}) \cos \theta \rangle, \end{aligned} \quad (10)$$

where $\mu' = 4\pi\mu$. Here, $\langle A \rangle = \frac{1}{2} \int_{-1}^1 A \, d \cos \theta$ represents the angular average of a quantity A that is a function of $\cos \theta$. In the next Section, we analyze the behaviors of neutrino oscillations based on the motion of the polarization vectors governed by Eq. (9). The z -components of polarization vectors include information of numbers of neutrinos. The finite value of C changes the length of the neutrino polarization vector. From Eq. (9), we can derive the equation of motion of the angled averaged length of polarization vectors,

$$\begin{aligned} \frac{d}{dt} \langle |P|^2 \rangle &= -2C (\langle |P|^2 \rangle - |\langle P \rangle|^2), \\ \frac{d}{dt} \langle |\bar{P}|^2 \rangle &= -2C (\langle |\bar{P}|^2 \rangle - |\langle \bar{P} \rangle|^2). \end{aligned} \quad (11)$$

The right hand sides of Eq. (11) vanish when the deviations in the angular distributions of neutrino polarization vector and that of antineutrinos disappear. The Eq. (11) implies that the distributions of polarization vectors become isotropic in equilibrium states of fast flavor conversions owing to collision effects. Furthermore, the Boltzmann collision changes the direction of emitted neutrinos, so that, in general, the $\text{Tr}\rho$ and $\text{Tr}\bar{\rho}$ are no longer invariant during flavor conversions even though the total neutrino numbers $2\langle \text{Tr}\rho \rangle$ and $2\langle \text{Tr}\bar{\rho} \rangle$ are conserved. The time evolution of these traces of density matrices can be solved analytically. In the case of initial distribution as shown in Eq. (7), the trace of neutrino density matrix does not evolve ($\text{Tr}\rho = 0.5$). On the other hand, the value of $\text{Tr}\bar{\rho}$ exponentially approach to that of $\langle \text{Tr}\bar{\rho} \rangle (= 0.4857)$ irrespective of scattering angle θ and the angular dependence finally disappears in equilibrium.

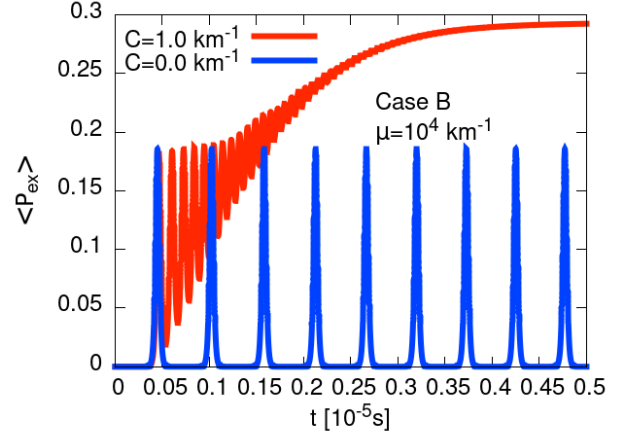


FIG. 1. The time evolution of transition probability $\langle P_{ex} \rangle$ with (red) and without (blue) the collision terms.

III. RESULTS

The overall evolution of angle averaged transition probability $\langle P_{ex} \rangle$ [73] is shown in Fig. 1. In our numerical setup, the trace of neutrino density matrix is invariant during flavor conversions ($\text{Tr}\rho = 0.5$), so that the $\langle P_{ex} \rangle$ is described by

$$\langle P_{ex} \rangle = \frac{1}{2} \left(1 - \frac{\langle P_z \rangle}{\langle P_z \rangle_{\text{ini}}} \right), \quad (12)$$

where $\langle P_z \rangle_{\text{ini}}$ is the initial value of $\langle P_z \rangle$, 0.5. In the case of $C = 0 \text{ km}^{-1}$ (blue line), the periodic structure of fast flavor conversions is confirmed. On the other hand, in the case of $C = 1 \text{ km}^{-1}$ (red line), flavor conversions are enhanced by the collision terms and the transition probability reaches an equilibrium value. Properties of fast flavor conversions in our calculation are consistent with results in Ref. [73] (see the Case B of Fig. 2 in the paper) except for the time scale of flavor conversions. The probability in Fig. 1 becomes large when $t > 0.05 \times 10^{-5} \text{ s}$ in both cases. The flavor conversions in Fig. 1 evolve faster than those of calculations in Ref. [73]. Such discrepancy in the time scale of flavor conversions is also reported in QKE-MC simulations [79]. This issue might be related to the strength of the initial perturbation. Since we imposed $\sim 10^{-8}$ random seed, the first peak in $\langle P_{ex} \rangle$ may arise faster.

The dynamics of fast flavor conversions is mainly divided by three epochs such as the linear evolution phase, the limit cycle phase, and the relaxation phase. The fast flavor conversions are enhanced in the limit cycle phase owing to the collision effect. The distribution of neutrinos finally become isotropic in the relaxation phase when the evolution time is comparable with the time scale of the collision term ($ct \sim C^{-1}$), where c is the speed of light. Hereafter we omit c when we convert timescale to length scale.

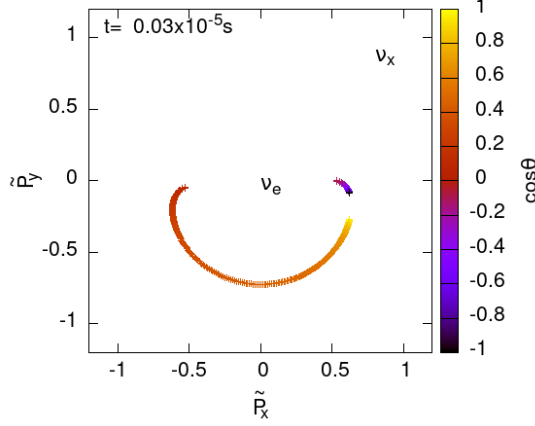


FIG. 2. The map of normalized neutrino polarization vector (\tilde{P}_x, \tilde{P}_y) in the linear evolution phase ($t = 0.03 \times 10^{-5}$ s). The normalized polarization vector is defined in Eq. (13).

A. Linear evolution phase

We call the epoch before reaching the first peak in $\langle P_{ex} \rangle$ linear evolution phase. In this early phase of fast flavor conversions ($t < 0.05 \times 10^{-5}$ s), the instability of flavor conversions appears near the ELN crossing in the initial distributions of ν_e and $\bar{\nu}_e$ ($\cos \theta \sim 0.5$). As shown in Fig. 1, collision effects are negligible in the linear evolution phase because of the large time scale of the collision terms ($t \ll C^{-1}$), so that flavor conversions without and with collision terms are almost equivalent. Here, we use time snapshots of neutrino polarization vectors with $C = 1 \text{ km}^{-1}$ at $t = 0.03 \times 10^{-5}$ s to study behaviors of fast flavor conversions during the linear phase.

Fig. 2 shows a map of normalized neutrino polarization vectors on the $\tilde{P}_x - \tilde{P}_y$ plane at $t = 0.03 \times 10^{-5}$ s. In this figure, for the convenience to see a polarization vector in the case of a small transition probability, the polarization vector is normalized as

$$\begin{aligned} \tilde{P}_x &= \left(1 + \frac{\log_{10} P_R / |P|}{15}\right) \cos(P_\phi), \\ \tilde{P}_y &= \left(1 + \frac{\log_{10} P_R / |P|}{15}\right) \sin(P_\phi), \end{aligned} \quad (13)$$

where $P_R = \sqrt{P_x^2 + P_y^2}$ and $P_\phi = \tan^{-1}(P_y/P_x)$ (in this paper, inverse tangent is calculated by `atan2` function in C++). At first, all neutrino polarization vectors lie in the z -axis ($(0, 0)$ in Fig. 2). As the calculation time has passed, the polarization vector begins a spiral motion around the z -axis increasing the value of P_R .

The dynamics of the polarization can be understood in cylindrical coordinate (R, ϕ, z) as follows. First we need to define and explain some variables. The quantity P_ϕ represents a phase of polarization vector on the $\tilde{P}_x - \tilde{P}_y$ plane. In negative value of $\cos \theta$, the motions of polariza-

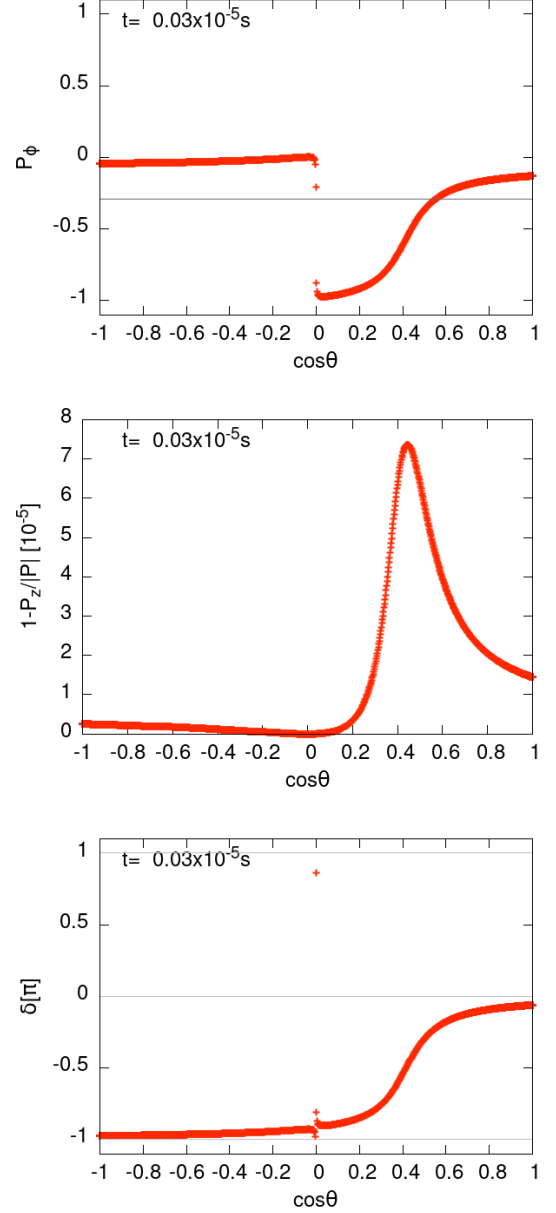


FIG. 3. Polarization vector at $t = 0.03 \times 10^{-5}$ s. Top: The angular distribution of the phase $P_\phi = \tan^{-1}(P_y/P_x)$. The gray line is the phase of averaged polarization vector, $\langle P \rangle_\phi = \tan^{-1}(\langle P_y \rangle / \langle P_x \rangle)$. Middle: The angular distribution of $1 - P_z/|P|$ in the unit of 10^{-5} . Bottom: The angular distribution of the phase difference δ . The definition of the δ is given in Eq. (14). The gray lines indicate 1, 0, -1 [π].

tion vectors synchronize with each other, which results in the same value of P_ϕ in the top panel of Fig. 3. On the other hand, the phase P_ϕ is distributed broadly in the case of $\cos \theta > 0$. The phase of $\cos \theta > 0.6$ is close to that of $\cos \theta < 0$. The P_ϕ becomes opposite phase in $0 < \cos \theta < 0.2$. The value of P_R becomes small around $\cos \theta \sim 0$, so that $\theta = \pi/2$ can be regarded as a singular point for P_ϕ . We discuss the reason why the P_R is small

around $\cos\theta = 0$ in Sec. III C. The z -component of the neutrino polarization vector is related to the transition probability. According to Eq. (12), the transition probability increases as the value of P_z decreases. The middle panel of Fig. 3 shows the distribution of $1 - P_z/|P|$ at $t = 0.03 \times 10^{-5}$ s. The flavor conversions do not proceed in $\cos\theta < 0.2$. However, the flavor conversions become prominent in $\cos\theta \sim 0.4$ that is close to the angle of the ELN crossing ($\cos\theta \sim 0.5$) in the initial distributions. Here, we define the phase difference between \mathbf{P} and the polarization vector of neutrino Hamiltonian \mathbf{H} on the x - y plane,

$$\begin{aligned} H_R &= \sqrt{H_x^2 + H_y^2}, \\ \delta &= P_\phi - H_\phi, \end{aligned} \quad (14)$$

where $\mathbf{H} = \omega\mathbf{B} + \mu'\mathbf{D}_0 - \mu'\cos\theta\mathbf{D}_1$ is the polarization vector of neutrino Hamiltonian and $H_\phi = \tan^{-1}(H_y/H_x)$ is the phase of \mathbf{H} on the x - y plane. The bottom panel of Fig. 3 shows the phase difference δ in Eq. (14) at $t = 0.03 \times 10^{-5}$ s. The phase difference δ is close to $-\pi$ in $\cos\theta < 0$ and $0 < \cos\theta < 0.2$. The jump of δ around $\cos\theta \sim 0$ reflects that of P_ϕ in the top panel of Fig. 3.

The evolution of P_z is related to the phase difference δ . In the linear evolution phase, the contribution of collision term is negligible, so that the time evolution of P_z is derived from Eq. (9),

$$\frac{d}{dt}P_z \sim H_x P_y - H_y P_x = H_R P_R \sin\delta. \quad (15)$$

The value of $\sin\delta$ in Eq. (15) is negligible when the direction of $\mathbf{P}_R = (P_x, P_y)$ is parallel ($\delta = 0$) or antiparallel ($\delta = \pm\pi$) to that of $\mathbf{H}_R = (H_x, H_y)$ on the x - y plane. At $t = 0.03 \times 10^{-5}$ s, the value of $|\sin\delta|$ is no longer negligible in $\cos\theta > 0.2$ and becomes maximum in $\cos\theta \sim 0.4$ (see the bottom panel of Fig. 3), so that fast flavor conversions proceed prominently in $\cos\theta \sim 0.4$ as shown in the middle panel of Fig. 3.

Several studies connect the dynamics of neutrino oscillation with the synchronization phenomena [88–90]. The evolution of the phase of polarization vector can be interpreted in the framework of the Kuramoto model [91], i.e.,

$$\frac{d\phi_i}{dt} = \omega_i + \frac{K}{N} \sum_{j=1}^N \sin(\phi_j - \phi_i), \quad (16)$$

where ϕ_i is the phase of i -th oscillator, which rotates with the frequency, ω_i . The total number of the oscillators is N and K is the coupling constant. Sufficiently high K makes synchronization, i.e., all ϕ_i rotates with the same frequency irrespective to the original ω_i . In the context of neutrino oscillation, this is a trivial equilibrium and no flavor conversions happen. The flavor conversion is expected when K becomes slightly lower, and the perfect synchronization is broken [89].

In our case, the strong coupling constant, μ , tries to synchronize the phase, and the phase is partially synchronized: the polarization vector at $\cos\theta > 0.6$ and $\cos\theta < 0$ rotates with the same phase (see Fig. 3 top panel). Due to the angular distribution with ELN crossing, that at $0 < \cos\theta < 0.2$ rotates with the opposite phase. The deviation from the synchronization at $\cos\theta \sim 0.4$ plays an essential role in the flavor conversion. As Ref. [89], the synchronization and small deviation from it govern the system.

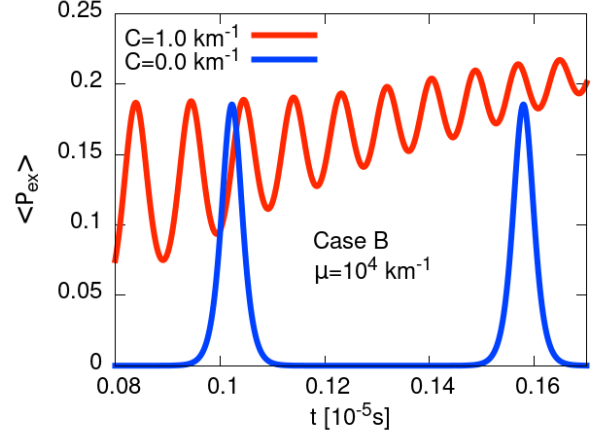


FIG. 4. Enlarge view of Fig. 1 in the limit cycle phase.

B. Limit cycle phase

Here, we define the limit cycle phase as the period from the linear evolution phase until $\langle P_{ex} \rangle$ settles down to its equilibrium value. Fig. 4 shows an enlarge view of Fig. 1 focusing on the flavor conversions in the limit cycle phase. In the case without collision terms (blue line), flavor conversions become periodic. On the other hand, in the case with collision term, the amplitude of the flavor conversion becomes gradually smaller and the transition probability is enhanced by collision effect (red line). In the limit cycle phase, the collision effect is no longer negligible in flavor conversions. We study the collision effect on the motion of neutrino polarization vectors in the limit cycle phase. The equation of motion of \mathbf{P} in Eq. (9) is decomposed by

$$\frac{d}{dt}P_z = H_R P_R \sin\delta - C(P_z - \langle P_z \rangle), \quad (17)$$

$$\frac{d}{dt}P_R = -H_R P_z \sin\delta - C(P_R - \langle P \rangle_R \cos\eta), \quad (18)$$

$$P_R \frac{dP_\phi}{dt} = -H_R P_z \cos\delta - C\langle P \rangle_R \sin\eta + P_R H_z \quad (19)$$

where H_R and δ are given in Eq. (14), and $\eta = P_\phi - \langle P \rangle_\phi$. Note that we first calculate average polarization $\langle P_x \rangle$ and $\langle P_y \rangle$, and then obtain $\langle P \rangle_R = \sqrt{\langle P_x \rangle^2 + \langle P_y \rangle^2}$

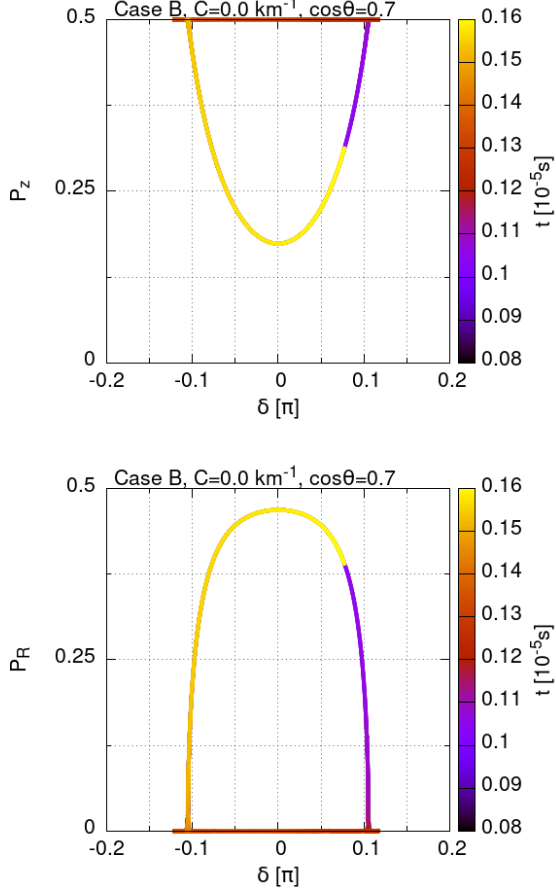


FIG. 5. Top: The time evolution of neutrino polarization vector ($\cos\theta = 0.7$) on the δ - P_z plane from 0.08×10^{-5} s to 0.16×10^{-5} s. Here, we set $C = 0 \text{ km}^{-1}$. At $t = 0.08 \times 10^{-5}$ s, δ is close to -0.1π . The polarization vector moves counterclockwise along the track. Bottom: The time evolution of polarization vector on the δ - P_R plane. The polarization vector moves clockwise along the track.

and $\langle P \rangle_\phi = \tan^{-1}(\langle P_y \rangle / \langle P_x \rangle)$. In general, $\langle P \rangle_R \neq \langle P_R \rangle$ and $\langle P \rangle_\phi \neq \langle P_\phi \rangle$, where the right hand sides are the average of P_R and P_ϕ , respectively.

Fig. 5 shows the time evolution of P_z and P_R at $\cos\theta = 0.7$ without the collision ($C = 0 \text{ km}^{-1}$) during t in 0.08 – 0.16 in the unit of 10^{-5} s, respectively. Without collision terms, the evolution tracks of polarization vectors in Fig. 5 are closed. The blue line in the top panel of Fig. 6 shows the evolution of δ without collision effect. At first, the value of δ is approximately -0.1π and almost constant. The value of δ increases dramatically around $t = 0.1 \times 10^{-5}$ s. According to the first terms on the right hand sides of Eqs. (17) and (18), the value of P_z (P_R) decreases (increases) when the δ is negative. In the case of positive δ , the value of P_z (P_R) increases (decreases). The perpendicular component is negligible ($P_R \sim 0$) and the z -component is constant ($P_z \sim 0.5$) at $t = (0.12\text{--}0.14) \times 10^{-5}$ s irrespective of decreasing δ .

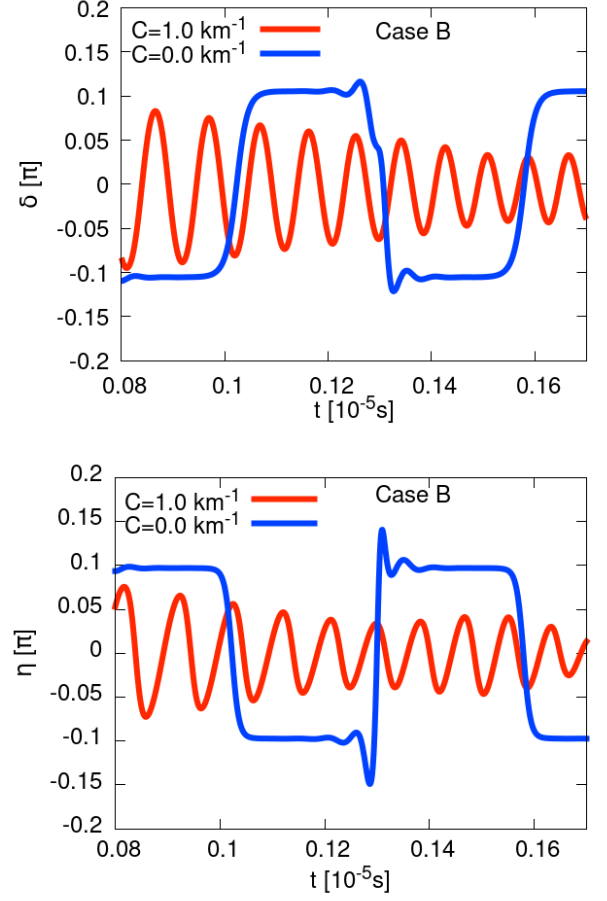


FIG. 6. Top: The time evolution of δ at $\cos\theta = 0.7$ in the limit cycle phase. Bottom: The time evolution of $\eta = P_\phi - \langle P \rangle_\phi$ at $\cos\theta = 0.7$ in the limit cycle phase. The blue (red) line shows the case of $C = 0 \text{ km}^{-1}$ ($C = 1 \text{ km}^{-1}$).

In such evolution phase, the small H_R suppresses the time evolution of P_z and P_R . Therefore, the polarization vector moves counterclockwise (clockwise) in Top panel (Bottom panel) of Fig. 5.

In the case with neutrino scatterings ($C = 1 \text{ km}^{-1}$), the evolution track of neutrino polarization vector is no longer a closed orbit but a “limit cycle” on the phase space because of the collision terms in Eqs.(17) and (18). The spiral motion of P_z and P_R at $\cos\theta = 0.7$ is shown in the top and bottom panels of Fig. 7, respectively. The value of δ is negative at $t = 0.08 \times 10^{-5}$ s (see the red line in the top panel of Fig. 6). By the first term on the right hand side of Eq. (17) (Eq. (18)), the value of P_z (P_R) decreases (increases) at first. On the other hand, in more later phase, δ becomes positive and P_z (P_R) increases (decreases).

The ranges of P_z and P_R changing in one cycle gradually decrease with each cycle. As shown in the red line of the top panel of Fig. 6, the oscillation amplitude of δ is decreasing and converging to zero. In the bottom panel, the evolution of η is also shown. Comparing the top and

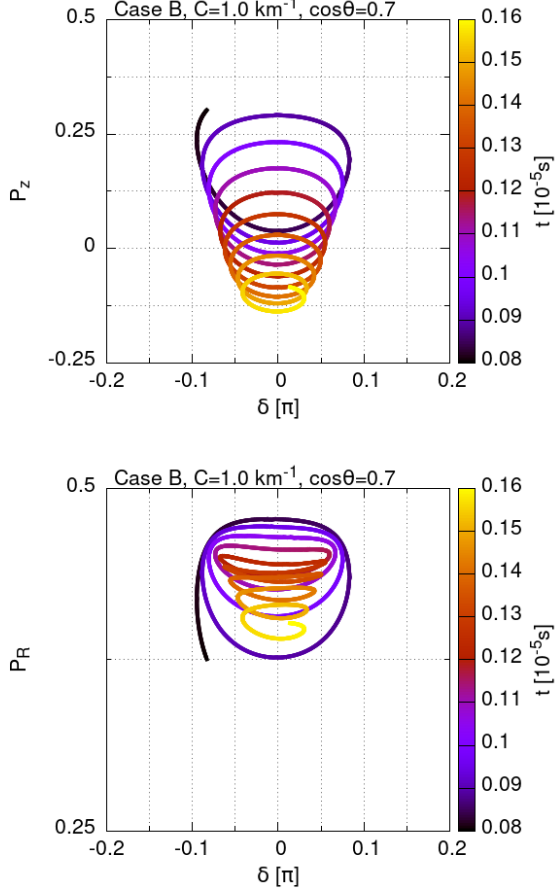


FIG. 7. Same to Fig. 5 but here, we consider the collision term ($C = 1 \text{ km}^{-1}$).

bottom panels, we found $\delta \sim -\eta$. Since the collision tries to align the polarization and decreases $|\eta| = |P_\phi - \langle P \rangle_\phi|$, $|\delta| \sim |\eta|$ is also expected to become smaller as time passes. After such synchronization between \mathbf{P}_R and \mathbf{H}_R , the first terms on the right hand side of Eqs. (17) and (18) are negligible and the transition probability $\langle P_{ex} \rangle$ no longer changes, which results in the end of the limit cycle phase.

One of the most interesting features of this model is that the mean value of P_z becomes smaller as time passes (e.g., top of Fig. 7). Fig. 8 shows $|\sin \delta|$. It is similar to Fig. 6, but we can compare positive δ and negative δ easily. In the case of $\cos \theta = 0.7$, the averaged $|\sin \delta|$ for negative δ is larger than that of positive δ in one cycle. In addition, the period with negative δ is slightly longer than the positive part. From Eq. (17), this imbalance of positive and negative δ leads to the gradual decrease of P_z . Note that this does not happen for all θ . In the case of $\cos \theta = 0.3$, on the other hand, the positive part is slightly larger than the positive part. This excess slightly increases the mean P_z (see the bottom of Fig. 10).

This imbalance comes from the highly non-linear dynamics of the partially synchronized oscillators, and it is

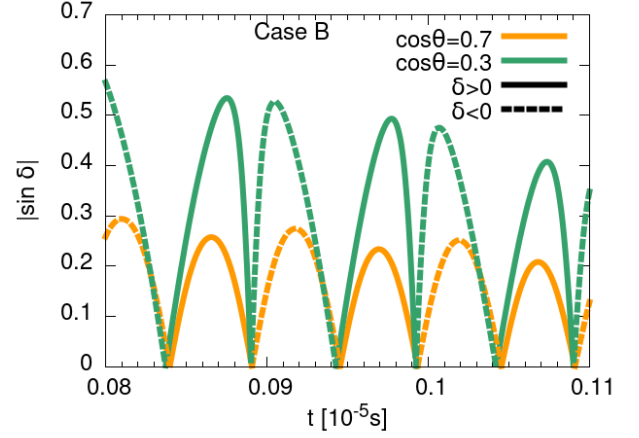


FIG. 8. The time evolution of $|\sin \delta|$ at $\cos \theta = 0.7$ (orange) and $\cos \theta = 0.3$ (green). For positive and negative δ , solid and dashed curve are used, respectively.

difficult to identify the mechanism to produce that. Here we show a hypothesis of the possible origin, focusing on the impact of the collision term on $\delta = P_\phi - H_\phi$. Note that other terms may also cause the imbalance. First we extract the impact of the collision term on the phase of the polarization vector: $\left. \frac{dP_\phi}{dt} \right|_{\text{coll}} = \left. \frac{dP_\phi}{dt} \right| - \left. \frac{dP_\phi}{dt} \right|_{C=0}$, where $\left. \frac{dP_\phi}{dt} \right|_{C=0}$ is obtained by substituting $C = 0$ in Eq. (19). Similarly, we consider the collisional part of δ : $\left. \frac{d\delta}{dt} \right|_{\text{coll}} = \frac{d\delta}{dt} - \left. \frac{d\delta}{dt} \right|_{C=0}$. This term could be well approximated as

$$\left. \frac{d\delta}{dt} \right|_{\text{coll}} = \left. \frac{dP_\phi}{dt} \right|_{\text{coll}} - \left. \frac{dH_\phi}{dt} \right|_{\text{coll}} \sim -C \left(\frac{\langle P \rangle_R}{P_R} \right) \sin \eta, \quad (20)$$

where we ignore the effect of the collision term in $\frac{dH_\phi}{dt}$ following Appendix A, and the collision term in Eq. (19) is extracted.

We demonstrate how the collision term violates the time symmetry using the schematic diagram of Fig. 9. Near $t = 0.0945 \times 10^{-5} \text{ s}$ in Fig. 8, δ of $\cos \theta = 0.7$ changes its sign from negative to positive, i.e., $\frac{d\delta}{dt} > 0$ (point A in the diagram). The collision term would decelerate δ when $t < 0.0945 \times 10^{-5} \text{ s}$ and $\delta < 0$ since the collision term, $\left. \frac{d\delta}{dt} \right|_{\text{coll}}$, is proportional to $-C \sin \eta \sim C \sin \delta < 0$ (here $\eta \sim -\delta$. see Fig. 6). Now $\frac{d\delta}{dt}$ is positive, and $\left. \frac{d\delta}{dt} \right|_{\text{coll}}$ is negative, then the evolution of δ would be decelerated by the collision (curve of D to A in the diagram). On the other hand, when $t > 0.0945 \times 10^{-5} \text{ s}$ and $\delta > 0$, the collision term accelerate the evolution of δ since $\frac{d\delta}{dt} > 0$ and $\left. \frac{d\delta}{dt} \right|_{\text{coll}}$ are both positive (Curve A-B in the diagram). These two effects make the duration in negative δ longer and positive δ shorter. Caveat that at $t = 0.099 \times 10^{-5} \text{ s}$, the collision term, vice versa, makes the duration in negative δ shorter and the duration in positive δ longer. Here

$\frac{d\delta}{dt} < 0$, and $\frac{d\delta}{dt}|_{\text{coll}} > 0$ (< 0) for positive (negative) δ in Curve B-C (C-D). We need more careful analysis for quantitative argument, which we keep in a future study as well as the possibility of other origin.

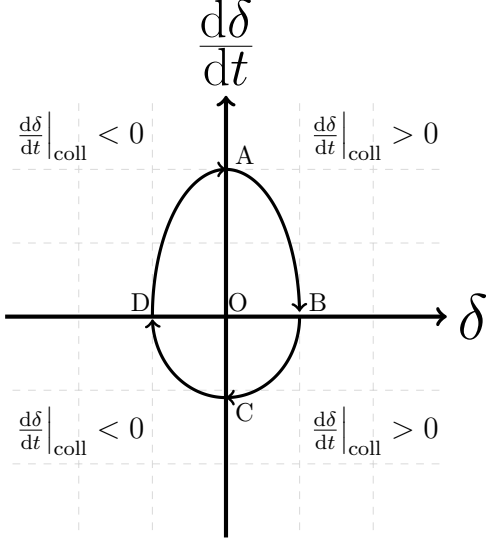


FIG. 9. Schematic diagram of the evolution of δ and $\frac{d\delta}{dt}$.

C. Relaxation phase

As implied in Eq. (11), the distributions of neutrinos affected by fast flavor conversions become isotropic in the relaxation phase ($t > C^{-1} = 0.33 \times 10^{-5}$ s). Up to the limit cycle phase, the fast flavor conversions are enhanced by collision effects and the transition probability $\langle P_{ex} \rangle$ does not change anymore as shown in Fig. 1. In the relaxation phase, the collision terms force all of polarization vectors to face z -axis keeping the value of $\langle P_{ex} \rangle$.

The top panel of Fig. 10 shows the time evolution of P_R in different angles and that of $\langle P \rangle_R$. Owing to the coupling of neutrino-neutrino interactions with neutrino scatterings, the value of P_R increases and saturates around $t \sim 0.1 \times 10^{-5}$ s. Note that the time of the first peak would depend on the initial perturbation. We impose $P_R \sim 10^{-8}$, initially. After the saturation, all of polarization vector starts to be parallel to the z -axis and the values of P_R are reduced to zero. The perpendicular component of $\cos \theta = 0$ (cyan curve) is small and the polarization vector always points near the z -axis. From Eqs.(9) and (10), equation of motions of \mathbf{D}_0 is described by

$$\frac{d}{dt} \mathbf{D}_0 = \omega (\langle \mathbf{P} \rangle + \langle \bar{\mathbf{P}} \rangle) \times \mathbf{B}. \quad (21)$$

The above equation of motion indicates that, in the case of a small vacuum frequency ($\omega t \ll 1$), \mathbf{D}_0 is almost con-

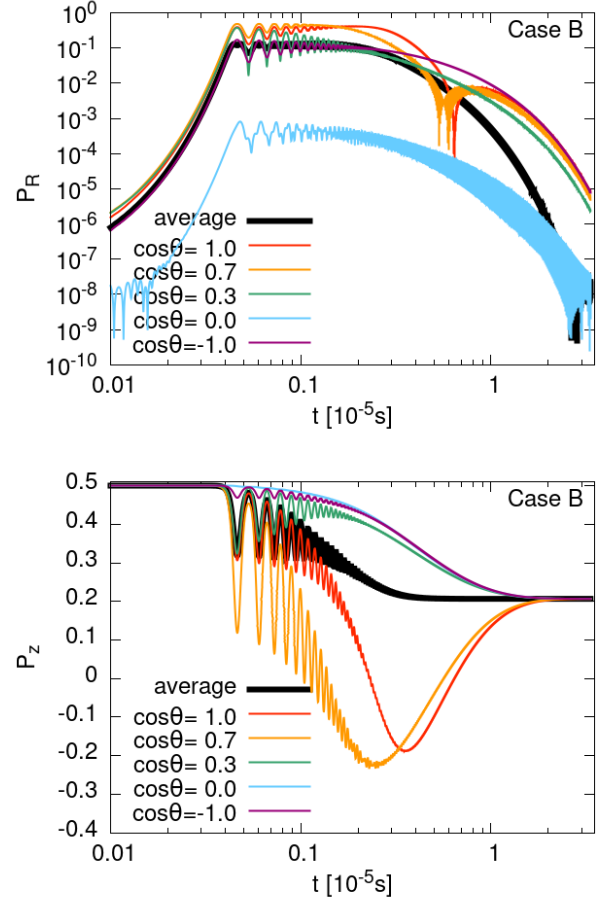


FIG. 10. Top: The time evolution of perpendicular component of neutrino polarization vectors at different angles (color curves), P_R , and that of angle averaged one (black), $\langle P \rangle_R$. Bottom: The time evolution of P_z at different angles and that of the angle averaged z -component $\langle P_z \rangle$. The red, orange, green, cyan, and purple curves show the case of $\cos \theta = 1, 0.7, 0.3, 0$ and -1 , respectively.

served during the flavor conversions and parallel to the z -axis. In addition, \mathbf{B} is also directed to the z -axis in the case of a small mixing angle ($\theta_v \ll 1$). Then, $\omega \mathbf{B} + \mu' \mathbf{D}_0$ in Eq. (9) is also parallel to the z -axis, so that the P_R is almost negligible at $\cos \theta = 0$. The evolution of P_z in different angles and that of $\langle P_z \rangle$ are shown in the bottom panel of Fig. 10. The fast flavor conversions increase the transition probability and induce different values of P_z depending on the scattering angle θ until the end of the limit cycle $t \sim C^{-1} = 0.33 \times 10^{-5}$ s. The flavor conversions in the limit cycle phase are especially enhanced at $\cos \theta = 0.7$ (orange curve) and $\cos \theta = 1$ (red curve) in the bottom panel of Fig. 10. Such enhancement of flavor conversions in forward scattered neutrinos is also confirmed in the middle panel of Fig. 11. However, after the limit cycle, the values of P_z in different angles (color curves) converge on the value of $\langle P_z \rangle$ (black curve). Then, the fast flavor conversions of neutrinos

have finished when $P_z = \langle P_z \rangle$ is satisfied in all of the scattering angles. Such behaviors of P_z can be understood by the equation of motion of P_z in the relaxation phase. Eq.(12) shows that the $\langle P_z \rangle$ is related to the transition probability as $\langle P_{ex} \rangle = 0.5 - \langle P_z \rangle$ in our numerical setup. As discussed in Sec. III B, the time evolution of $\langle P_{ex} \rangle$ reaches an equilibrium in the limit cycle phase owing to the synchronization between polarization vectors of neutrino density matrix and that of Hamiltonian ($\mathbf{P}_R \parallel \mathbf{H}_R$). Therefore, the value of δ is negligible and the value of $\langle P_z \rangle$ becomes constant before the relaxation phase. Then, the equation of motion of P_z in the relaxation phase is derived from Eq. (17),

$$\frac{d}{dt}P_z \sim -C(P_z - \langle P_z \rangle), \quad (22)$$

which explains the relaxation of P_z to $\langle P_z \rangle$ in all scattering angles at $t > C^{-1} = 0.33 \times 10^{-5} \text{ s}$ as shown in the bottom panel of Fig.10. Here, we discuss the relaxation of polarization vectors in neutrino sector, but the case of antineutrinos are similar. In the case of antineutrinos, the polarization vector $\bar{\mathbf{P}}$ is relaxed to $(0, 0, \langle \bar{P} \rangle)$ irrespective of the scattering angle θ .

The angular distributions of neutrinos after fast flavor conversions are shown in Fig. 11 bottom panel. As implied in Eq. (11), the angular dependence disappears in the distribution of neutrinos. The density matrices of neutrinos (antineutrinos) become diagonal because of the negligible $P_R(\bar{P}_R)$ and the finite $P_z(\bar{P}_z)$. The middle panel is taken at $t = 0.27 \times 10^{-5} \text{ s}$. Up to the limit cycle, the values of ρ_{ee} and $\bar{\rho}_{ee}$ depend on the scattering angle [73]. It looks similar to the stationary solution without collision [78]. However, such angular dependence disappear during the relaxation phase and the neutrino distribution becomes isotropic because of the collision effect. In Fig. 11 bottom panel, the value of ρ_{xx} (blue curve) is equal to that of $\bar{\rho}_{xx}$ (purple curve). Such correspondence can be explained by a conservation law below

$$\mathbf{B} \cdot \mathbf{D}_0 = \text{const.} \quad (23)$$

The above equation is derived from Eq. (21). In the case of small vacuum mixing angle, $\langle P_z \rangle - \langle \bar{P}_z \rangle$ is almost conserved according to Eq. (23). Furthermore the $\langle \text{Tr} \rho \rangle$ and $\langle \text{Tr} \bar{\rho} \rangle$ are time-independent quantities. Therefore, we can show that $\langle \rho_{xx} \rangle$ is almost equal to $\langle \bar{\rho}_{xx} \rangle$ at any time:

$$\begin{aligned} \langle \rho_{xx} \rangle - \langle \bar{\rho}_{xx} \rangle &= \frac{\langle \text{Tr} \rho \rangle}{2} - \frac{\langle \text{Tr} \bar{\rho} \rangle}{2} - \frac{\langle P_z \rangle}{2} + \frac{\langle \bar{P}_z \rangle}{2} \\ &\sim (\langle \rho_{xx} \rangle - \langle \bar{\rho}_{xx} \rangle)(t=0) \\ &= 0. \end{aligned} \quad (24)$$

After the relaxation phase, neutrino distribution becomes isotropic, so that $\rho_{xx} \sim \bar{\rho}_{xx}$ is satisfied in the end of the calculation as shown in Fig. 11.

Note that the appearance of the relaxation phase depends on the situation. The ELN crossing, considered

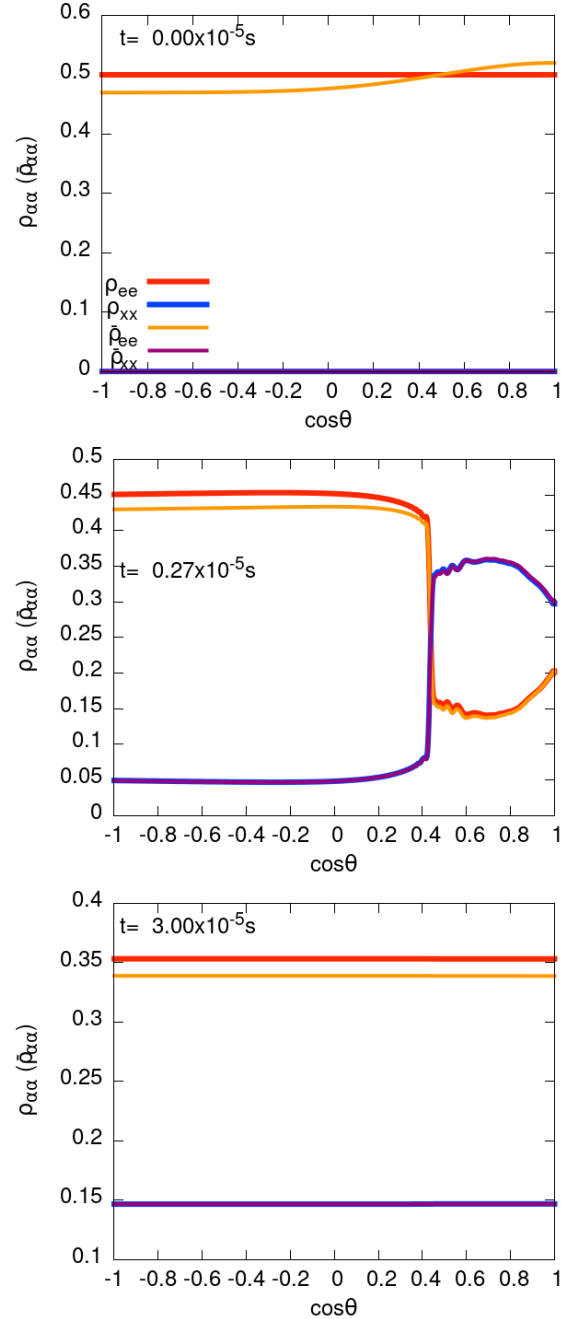


FIG. 11. Time snapshots of neutrino spectra. The initial ($t = 0 \text{ s}$), after limit cycle ($t = 0.27 \times 10^{-5} \text{ s}$), after the relaxation ($t = 3.00 \times 10^{-5} \text{ s}$) snapshots are taken, respectively. The distribution of ρ_{ee} , ρ_{xx} , $\bar{\rho}_{ee}$, and $\bar{\rho}_{xx}$ correspond to red, blue, orange, and purple curves, respectively.

here, typically appears above the neutrino sphere [67], and it means the opacity is less than one, i.e., $t < C^{-1}$. On the other hand, the ELN crossing in proto-neutron stars, opacity is larger than one, and the relaxation phase should be considered. In any case, the discussion here would be helpful to understand the role of the collision term.

IV. CONCLUSIONS

We calculate fast flavor conversions with collision effects of neutrino scatterings and analyze behaviors of the flavor conversions based on the dynamics of neutrino polarization vectors in cylindrical coordinate where we can easily access the information of the phase of rotation.

We find that the collision terms induce enhancement of flavor conversions and isotropization of neutrino distributions. In the linear phase, the instability of fast flavor conversions grows up around the ELN crossing where the phase difference δ takes an intermediate value in the range between 0 and $-\pi$. In the limit cycle phase, the evolution track of neutrino polarization vector without collision effects is closed, and flavor conversions show a periodic trend. On the other hand, with the collision terms, the evolution track of the neutrino polarization vector is no longer closed because of the decrease of $|\delta|$ in every cycle. The collision term breaks the symmetry between positive and negative δ , and the induced imbalance enhances the total transition probability. After the synchronization of neutrino polarization vectors, the value of δ finally converges to zero. At the end of the limit cycle, the evolution of $\langle P_{ex} \rangle$ settles down to equilibrium, and the distributions of neutrinos are dependent on the neutrino scattering angle. Such properties are well consistent with the results in Ref. [73]. However, in the relaxation phase, all of the neutrino polarization vectors align with the z -axis keeping the value of $\langle P_{ex} \rangle$. The distributions of neutrinos finally become isotropic after the relaxation phase. Such isotropic neutrino distributions after the fast flavor conversions are also confirmed in Ref. [75, 76].

Here, we remark on the uncertainties of our works. The behaviors of fast flavor conversions are sensitive to initial neutrino distributions, the strength of the vacuum frequency, and the number of neutrino flavors [73, 74]. In some cases, even without the collision terms, fast flavor conversions can decay and reach stationary solutions [75, 78]. The sensitivity of the numerical setup of fast flavor conversions to their behaviors is still uncertain. In our model, the angular dependence in collision term is completely ignored, but generally, the collision terms of neutrino scatterings should depend on the scattering angle of incoming and outgoing neutrinos [76]. The refinement of collision terms is necessary to more quantitatively reveal the effect of collision terms on fast flavor conversions. Furthermore, we focus on behaviors of fast flavor conversions of two flavor neutrinos for simplicity, but three flavors of neutrinos are required to predict the

reliable neutrino signal in explosive astrophysical sites.

ACKNOWLEDGMENTS

We thank E. Kokubo for fruitful discussion. This work was carried out under the auspices of the National Nuclear Security Administration of the U.S. Department of Energy at Los Alamos National Laboratory under Contract No. 89233218CNA000001. This study was supported in part by JSPS/MEXT KAKENHI Grant Numbers JP18H01212, JP17H06364, JP21H01088. This work is also supported by the NINS program for cross-disciplinary study (Grant Numbers 01321802 and 01311904) on Turbulence, Transport, and Heating Dynamics in Laboratory and Solar/Astrophysical Plasmas: "SoLaBo-X", and also by MEXT as "Program for Promoting researches on the Supercomputer Fugaku" (Toward a unified view of the universe: from large scale structures to planets, JPMXP1020200109) with JICFuS Numerical computations were carried out on PC cluster at the Center for Computational Astrophysics, National Astronomical Observatory of Japan.

Appendix A: The derivation of Eq.(20)

As discussed in Sec. III C, both \mathbf{D}_0 and \mathbf{B} are almost parallel to the z -axis when vacuum frequency and the mixing angle are small. In such a case, the polarization vector of neutrino Hamiltonian on the x - y plane is described by

$$H_x \sim -\mu' \cos \theta D_{1x}, \quad (\text{A1})$$

$$H_y \sim -\mu' \cos \theta D_{1y}, \quad (\text{A2})$$

where D_{1x} and D_{1y} are x and y components of \mathbf{D}_1 in Eq. (10). Then, the equation of motion of $H_i (i = x, y)$ is written as

$$\frac{dH_i}{dt} \sim \left. \frac{dH_i}{dt} \right|_{C=0} - CH_i, \quad (\text{A3})$$

where the first term on the right hand side of Eq. (A3) does not include the collision parameter C explicitly. From Eq. (A3), the time derivative of the phase H_ϕ is given by

$$\frac{dH_\phi}{dt} = -\frac{1}{H_R^2} \left(H_y \frac{dH_x}{dt} - H_x \frac{dH_y}{dt} \right) \sim \left. \frac{dH_\phi}{dt} \right|_{C=0}. \quad (\text{A4})$$

Finally, Eq. (20) is derived from Eqs. (19) and (A4).

[1] E. Vitagliano, I. Tamborra, and G. Raffelt, Grand Unified Neutrino Spectrum at Earth: Sources and Spectral Components, *Rev. Mod. Phys.* **92**, 45006 (2020),

[arXiv:1910.11878 \[astro-ph.HE\]](https://arxiv.org/abs/1910.11878).

[2] S. Horiuchi and J. P. Kneller, What can be learned from a future supernova neutrino detection?, *Journal of Physics*

- G: Nuclear and Particle Physics **45**, 043002 (2018).
- [3] H.-T. Janka, Neutrino Emission from Supernovae, in *Handbook of Supernovae*, 1966 (Springer International Publishing, Cham, 2017) pp. 1575–1604.
 - [4] A. Mirizzi, I. Tamborra, H.-T. Janka, N. Saviano, K. Scholberg, R. Bollig, L. Hudepohl, and S. Chakraborty, Supernova Neutrinos: Production, Oscillations and Detection, *Rivista del Nuovo Cimento* **39**, 1 (2015).
 - [5] L. Wolfenstein, Neutrino oscillations in matter, *Physical Review D* **17**, 2369 (1978).
 - [6] S. P. Mikheyev and A. Yu. Smirnov, Resonance Amplification of Oscillations in Matter and Spectroscopy of Solar Neutrinos, *Sov. J. Nucl. Phys.* **42**, 913 (1985), [305(1986)].
 - [7] H. Duan, G. M. Fuller, J. Carlson, and Y.-Z. Qian, Simulation of Coherent Non-Linear Neutrino Flavor Transformation in the Supernova Environment. 1. Correlated Neutrino Trajectories, *Phys. Rev. D* **74**, 105014 (2006), [arXiv:astro-ph/0606616 \[astro-ph\]](#).
 - [8] G. L. Fogli, E. Lisi, A. Marrone, and A. Mirizzi, Collective neutrino flavor transitions in supernovae and the role of trajectory averaging, *JCAP* **0712**, 010, [arXiv:0707.1998 \[hep-ph\]](#).
 - [9] B. Dasgupta, A. Mirizzi, I. Tamborra, and R. Tomas, Neutrino mass hierarchy and three-flavor spectral splits of supernova neutrinos, *Phys. Rev. D* **81**, 093008 (2010), [arXiv:1002.2943 \[hep-ph\]](#).
 - [10] H. Duan and A. Friedland, Self-induced suppression of collective neutrino oscillations in a supernova, *Phys. Rev. Lett.* **106**, 091101 (2011), [arXiv:1006.2359 \[hep-ph\]](#).
 - [11] A. Friedland, Self-refraction of supernova neutrinos: mixed spectra and three-flavor instabilities, *Phys. Rev. Lett.* **104**, 191102 (2010), [arXiv:1001.0996 \[hep-ph\]](#).
 - [12] A. Mirizzi and R. Tomas, Multi-angle effects in self-induced oscillations for different supernova neutrino fluxes, *Phys. Rev. D* **84**, 033013 (2011), [arXiv:1012.1339 \[hep-ph\]](#).
 - [13] J. F. Cherry, G. M. Fuller, J. Carlson, H. Duan, and Y.-Z. Qian, Multi-Angle Simulation of Flavor Evolution in the Neutrino Neutronization Burst From an O-Ne-Mg Core-Collapse Supernova, *Phys. Rev. D* **82**, 085025 (2010), [arXiv:1006.2175 \[astro-ph.HE\]](#).
 - [14] S. Chakraborty, T. Fischer, A. Mirizzi, N. Saviano, and R. Tomas, Analysis of matter suppression in collective neutrino oscillations during the supernova accretion phase, *Phys. Rev. D* **84**, 025002 (2011), [arXiv:1105.1130 \[hep-ph\]](#).
 - [15] M.-R. Wu, Y.-Z. Qian, G. Martinez-Pinedo, T. Fischer, and L. Huther, Effects of neutrino oscillations on nucleosynthesis and neutrino signals for an 18 M supernova model, *Phys. Rev. D* **91**, 065016 (2015), [arXiv:1412.8587 \[astro-ph.HE\]](#).
 - [16] V. Cirigliano, M. W. Paris, and S. Shalgar, Effect of collisions on neutrino flavor inhomogeneity in a dense neutrino gas, *Phys. Lett. B* **774**, 258 (2017), [arXiv:1706.07052 \[hep-ph\]](#).
 - [17] V. Cirigliano, M. Paris, and S. Shalgar, Collective neutrino oscillations with the halo effect in single-angle approximation, *JCAP* **11**, 019, [arXiv:1807.07070 \[hep-ph\]](#).
 - [18] H. Sasaki, T. Kajino, T. Takiwaki, T. Hayakawa, A. B. Balantekin, and Y. Pehlivan, Possible effects of collective neutrino oscillations in three-flavor multiangle simulations of supernova νp processes, *Phys. Rev. D* **96**, 043013 (2017), [arXiv:1707.09111 \[astro-ph.HE\]](#).
 - [19] H. Sasaki, T. Takiwaki, S. Kawagoe, S. Horiuchi, and K. Ishidoshiro, Detectability of Collective Neutrino Oscillation Signatures in the Supernova Explosion of a $8.8 M_{\odot}$ star, *Phys. Rev. D* **101**, 063027 (2020), [arXiv:1907.01002 \[astro-ph.HE\]](#).
 - [20] J. F. Cherry, G. M. Fuller, S. Horiuchi, K. Kotake, T. Takiwaki, and T. Fischer, Time of Flight and Supernova Progenitor Effects on the Neutrino Halo, *Phys. Rev. D* **102**, 023022 (2020), [arXiv:1912.11489 \[astro-ph.HE\]](#).
 - [21] M. Zaizen, J. F. Cherry, T. Takiwaki, S. Horiuchi, K. Kotake, H. Umeda, and T. Yoshida, Neutrino halo effect on collective neutrino oscillation in iron core-collapse supernova model of a $9.6 M_{\text{Solar}}$ star, *J. Cosmology Astropart. Phys.* **2020**, 011 (2020), [arXiv:1908.10594 \[astro-ph.HE\]](#).
 - [22] M. Zaizen, S. Horiuchi, T. Takiwaki, K. Kotake, T. Yoshida, H. Umeda, and J. F. Cherry, Three-flavor collective neutrino conversions with multi-azimuthal-angle instability in an electron-capture supernova model, *Phys. Rev. D* **103**, 063008 (2021), [arXiv:2011.09635 \[astro-ph.HE\]](#).
 - [23] A. Malkus, A. Friedland, and G. C. McLaughlin, Matter-Neutrino Resonance Above Merging Compact Objects, *arXiv e-prints*, [arXiv:1403.5797](#) (2014), [arXiv:1403.5797 \[hep-ph\]](#).
 - [24] A. Malkus, G. C. McLaughlin, and R. Surman, Symmetric and Standard Matter-Neutrino Resonances Above Merging Compact Objects, *Phys. Rev. D* **93**, 045021 (2016), [arXiv:1507.00946 \[hep-ph\]](#).
 - [25] M.-R. Wu, H. Duan, and Y.-Z. Qian, Physics of neutrino flavor transformation through matter–neutrino resonances, *Phys. Lett. B* **752**, 89 (2016), [arXiv:1509.08975 \[hep-ph\]](#).
 - [26] Y.-L. Zhu, A. Perego, and G. C. McLaughlin, Matter Neutrino Resonance Transitions above a Neutron Star Merger Remnant, *Phys. Rev. D* **94**, 105006 (2016), [arXiv:1607.04671 \[hep-ph\]](#).
 - [27] M. Frensel, M.-R. Wu, C. Volpe, and A. Perego, Neutrino Flavor Evolution in Binary Neutron Star Merger Remnants, *Phys. Rev. D* **95**, 023011 (2017), [arXiv:1607.05938 \[astro-ph.HE\]](#).
 - [28] A. Chatelain and C. Volpe, Helicity coherence in binary neutron star mergers and non-linear feedback, *Phys. Rev. D* **95**, 043005 (2017), [arXiv:1611.01862 \[hep-ph\]](#).
 - [29] J. Y. Tian, A. V. Patwardhan, and G. M. Fuller, Neutrino Flavor Evolution in Neutron Star Mergers, *Phys. Rev. D* **96**, 043001 (2017), [arXiv:1703.03039 \[astro-ph.HE\]](#).
 - [30] A. Vlasenko and G. C. McLaughlin, Matter-neutrino resonance in a multiple neutrino bulb model, *Phys. Rev. D* **97**, 083011 (2018), [arXiv:1801.07813 \[astro-ph.HE\]](#).
 - [31] S. Shalgar, Multi-angle calculation of the matter-neutrino resonance near an accretion disk, *JCAP* **02**, 010, [arXiv:1707.07692 \[hep-ph\]](#).
 - [32] V. A. Kostelecky, J. T. Pantaleone, and S. Samuel, Neutrino oscillation in the early universe, *Phys. Lett. B* **315**, 46 (1993).
 - [33] A. D. Dolgov, S. H. Hansen, S. Pastor, S. T. Petcov, G. G. Raffelt, and D. V. Semikoz, Cosmological bounds on neutrino degeneracy improved by flavor oscillations, *Nucl. Phys. B* **632**, 363 (2002), [arXiv:hep-ph/0201287](#).
 - [34] Y. Y. Y. Wong, Analytical treatment of neutrino asymmetry equilibration from flavor oscillations in the early universe, *Phys. Rev. D* **66**, 025015 (2002), [arXiv:hep-ph/0203180](#).

- [35] L. Johns, M. Mina, V. Cirigliano, M. W. Paris, and G. M. Fuller, Neutrino flavor transformation in the lepton-asymmetric universe, *Phys. Rev. D* **94**, 083505 (2016), [arXiv:1608.01336 \[hep-ph\]](#).
- [36] P. F. de Salas and S. Pastor, Relic neutrino decoupling with flavour oscillations revisited, *JCAP* **07**, 051, [arXiv:1606.06986 \[hep-ph\]](#).
- [37] T. Hasegawa, N. Hiroshima, K. Kohri, R. S. L. Hansen, T. Tram, and S. Hannestad, MeV-scale reheating temperature and thermalization of oscillating neutrinos by radiative and hadronic decays of massive particles, *JCAP* **12**, 012, [arXiv:1908.10189 \[hep-ph\]](#).
- [38] R. S. L. Hansen, S. Shalgar, and I. Tamborra, Neutrino flavor mixing breaks isotropy in the early universe, *JCAP* **07**, 017, [arXiv:2012.03948 \[astro-ph.CO\]](#).
- [39] G. Martinez-Pinedo, B. Ziebarth, T. Fischer, and K. Langanke, Effect of collective neutrino flavor oscillations on vp-process nucleosynthesis, *Eur. Phys. J. A* **47**, 98 (2011), [arXiv:1105.5304 \[astro-ph.SR\]](#).
- [40] E. Pllumbi, I. Tamborra, S. Wanajo, H.-T. Janka, and L. Hüdepohl, Impact of neutrino flavor oscillations on the neutrino-driven wind nucleosynthesis of an electron-capture supernova, *Astrophys. J.* **808**, 188 (2015), [arXiv:1406.2596 \[astro-ph.SR\]](#).
- [41] Z. Xiong, A. Sieverding, M. Sen, and Y.-Z. Qian, Potential Impact of Fast Flavor Oscillations on Neutrino-driven Winds and Their Nucleosynthesis, *Astrophys. J.* **900**, 144 (2020), [arXiv:2006.11414 \[astro-ph.HE\]](#).
- [42] M.-R. Wu, I. Tamborra, O. Just, and H.-T. Janka, Imprints of neutrino-pair flavor conversions on nucleosynthesis in ejecta from neutron-star merger remnants, *Phys. Rev. D* **96**, 123015 (2017), [arXiv:1711.00477 \[astro-ph.HE\]](#).
- [43] M. George, M.-R. Wu, I. Tamborra, R. Ardevol-Pulpillo, and H.-T. Janka, Fast neutrino flavor conversion, ejecta properties, and nucleosynthesis in newly-formed hypermassive remnants of neutron-star mergers, *Phys. Rev. D* **102**, 103015 (2020), [arXiv:2009.04046 \[astro-ph.HE\]](#).
- [44] I. Tamborra and S. Shalgar, New Developments in Flavor Evolution of a Dense Neutrino Gas, *arXiv e-prints*, [arXiv:2011.01948 \(2020\)](#), [arXiv:2011.01948 \[astro-ph.HE\]](#).
- [45] R. F. Sawyer, Speed-up of neutrino transformations in a supernova environment, *Phys. Rev. D* **72**, 045003 (2005), [arXiv:hep-ph/0503013](#).
- [46] R. F. Sawyer, The multi-angle instability in dense neutrino systems, *Phys. Rev. D* **79**, 105003 (2009), [arXiv:0803.4319 \[astro-ph\]](#).
- [47] R. F. Sawyer, Neutrino cloud instabilities just above the neutrino sphere of a supernova, *Phys. Rev. Lett.* **116**, 081101 (2016), [arXiv:1509.03323 \[astro-ph.HE\]](#).
- [48] B. Dasgupta, A. Mirizzi, and M. Sen, Fast neutrino flavor conversions near the supernova core with realistic flavor-dependent angular distributions, *JCAP* **02**, 019, [arXiv:1609.00528 \[hep-ph\]](#).
- [49] I. Izaguirre, G. Raffelt, and I. Tamborra, Fast Pairwise Conversion of Supernova Neutrinos: A Dispersion-Relation Approach, *Phys. Rev. Lett.* **118**, 021101 (2017), [arXiv:1610.01612 \[hep-ph\]](#).
- [50] S. Chakraborty, R. S. Hansen, I. Izaguirre, and G. Raffelt, Self-induced neutrino flavor conversion without flavor mixing, *JCAP* **03**, 042, [arXiv:1602.00698 \[hep-ph\]](#).
- [51] F. Capozzi, B. Dasgupta, E. Lisi, A. Marrone, and A. Mirizzi, Fast flavor conversions of supernova neutrinos: Classifying instabilities via dispersion relations, *Phys. Rev. D* **96**, 043016 (2017), [arXiv:1706.03360 \[hep-ph\]](#).
- [52] S. Abbar, H. Duan, K. Sumiyoshi, T. Takiwaki, and M. C. Volpe, On the occurrence of fast neutrino flavor conversions in multidimensional supernova models, *Phys. Rev. D* **100**, 043004 (2019), [arXiv:1812.06883 \[astro-ph.HE\]](#).
- [53] S. Abbar, H. Duan, K. Sumiyoshi, T. Takiwaki, and M. C. Volpe, Fast Neutrino Flavor Conversion Modes in Multidimensional Core-collapse Supernova Models: the Role of the Asymmetric Neutrino Distributions, *Phys. Rev. D* **101**, 043016 (2020), [arXiv:1911.01983 \[astro-ph.HE\]](#).
- [54] R. Glas, H. T. Janka, F. Capozzi, M. Sen, B. Dasgupta, A. Mirizzi, and G. Sigl, Fast Neutrino Flavor Instability in the Neutron-star Convection Layer of Three-dimensional Supernova Models, *Phys. Rev. D* **101**, 063001 (2020), [arXiv:1912.00274 \[astro-ph.HE\]](#).
- [55] M. Delfan Azari, S. Yamada, T. Morinaga, H. Nagakura, S. Furusawa, A. Harada, H. Okawa, W. Iwakami, and K. Sumiyoshi, Fast collective neutrino oscillations inside the neutrino sphere in core-collapse supernovae, *Phys. Rev. D* **101**, 023018 (2020), [arXiv:1910.06176 \[astro-ph.HE\]](#).
- [56] M. Delfan Azari, S. Yamada, T. Morinaga, W. Iwakami, H. Okawa, H. Nagakura, and K. Sumiyoshi, Linear Analysis of Fast-Pairwise Collective Neutrino Oscillations in Core-Collapse Supernovae based on the Results of Boltzmann Simulations, *Phys. Rev. D* **99**, 103011 (2019), [arXiv:1902.07467 \[astro-ph.HE\]](#).
- [57] T. Morinaga, H. Nagakura, C. Kato, and S. Yamada, Fast neutrino-flavor conversion in the preshock region of core-collapse supernovae, *Phys. Rev. Res.* **2**, 012046 (2020), [arXiv:1909.13131 \[astro-ph.HE\]](#).
- [58] H. Nagakura, T. Morinaga, C. Kato, and S. Yamada, Fast-pairwise Collective Neutrino Oscillations Associated with Asymmetric Neutrino Emissions in Core-collapse Supernovae, *ApJ* **886**, 139 (2019), [arXiv:1910.04288 \[astro-ph.HE\]](#).
- [59] S. Abbar, F. Capozzi, R. Glas, H. T. Janka, and I. Tamborra, On the characteristics of fast neutrino flavor instabilities in three-dimensional core-collapse supernova models, *Phys. Rev. D* **103**, 063033 (2021), [arXiv:2012.06594 \[astro-ph.HE\]](#).
- [60] M.-R. Wu and I. Tamborra, Fast neutrino conversions: Ubiquitous in compact binary merger remnants, *Phys. Rev. D* **95**, 103007 (2017), [arXiv:1701.06580 \[astro-ph.HE\]](#).
- [61] X. Li and D. M. Siegel, Neutrino Fast Flavor Conversions in Neutron-Star Postmerger Accretion Disks, *Phys. Rev. Lett.* **126**, 251101 (2021), [arXiv:2103.02616 \[astro-ph.HE\]](#).
- [62] S. Abbar and H. Duan, Fast neutrino flavor conversion: roles of dense matter and spectrum crossing, *Phys. Rev. D* **98**, 043014 (2018), [arXiv:1712.07013 \[hep-ph\]](#).
- [63] S. Abbar, Searching for Fast Neutrino Flavor Conversion Modes in Core-collapse Supernova Simulations, *JCAP* **05**, 027, [arXiv:2003.00969 \[astro-ph.HE\]](#).
- [64] H. Nagakura and L. Johns, New method for detecting fast neutrino flavor conversions in core-collapse supernova models with two-moment neutrino transport, *Phys. Rev. D* **104**, 063014 (2021), [arXiv:2106.02650 \[astro-ph.HE\]](#).

- [65] L. Johns and H. Nagakura, Fast flavor instabilities and the search for neutrino angular crossings, *Phys. Rev. D* **103**, 123012 (2021), [arXiv:2104.04106 \[hep-ph\]](#).
- [66] F. Capozzi, S. Abbar, R. Bollig, and H. T. Janka, Fast neutrino flavor conversions in one-dimensional core-collapse supernova models with and without muon creation, *Phys. Rev. D* **103**, 063013 (2021), [arXiv:2012.08525 \[astro-ph.HE\]](#).
- [67] H. Nagakura, L. Johns, A. Burrows, and G. M. Fuller, Where, when and why: occurrence of fast-pairwise collective neutrino oscillation in three-dimensional core-collapse supernova models, *arXiv e-prints*, [arXiv:2108.07281](#) (2021), [arXiv:2108.07281 \[astro-ph.HE\]](#).
- [68] B. Dasgupta and M. Sen, Fast Neutrino Flavor Conversion as Oscillations in a Quartic Potential, *Phys. Rev. D* **97**, 023017 (2018), [arXiv:1709.08671 \[hep-ph\]](#).
- [69] S. Abbar and M. C. Volpe, On Fast Neutrino Flavor Conversion Modes in the Nonlinear Regime, *Phys. Lett. B* **790**, 545 (2019), [arXiv:1811.04215 \[astro-ph.HE\]](#).
- [70] F. Capozzi, B. Dasgupta, A. Mirizzi, M. Sen, and G. Sigl, Collisional triggering of fast flavor conversions of supernova neutrinos, *Phys. Rev. Lett.* **122**, 091101 (2019), [arXiv:1808.06618 \[hep-ph\]](#).
- [71] L. Johns, H. Nagakura, G. M. Fuller, and A. Burrows, Neutrino oscillations in supernovae: angular moments and fast instabilities, *Phys. Rev. D* **101**, 043009 (2020), [arXiv:1910.05682 \[hep-ph\]](#).
- [72] S. Shalgar and I. Tamborra, Dispelling a myth on dense neutrino media: fast pairwise conversions depend on energy, *JCAP* **01**, 014, [arXiv:2007.07926 \[astro-ph.HE\]](#).
- [73] S. Shalgar and I. Tamborra, A change of direction in pairwise neutrino conversion physics: The effect of collisions, *Phys. Rev. D* **103**, 063002 (2021), [arXiv:2011.00004 \[astro-ph.HE\]](#).
- [74] S. Shalgar and I. Tamborra, Three flavor revolution in fast pairwise neutrino conversion, *Phys. Rev. D* **104**, 023011 (2021), [arXiv:2103.12743 \[hep-ph\]](#).
- [75] J. D. Martin, C. Yi, and H. Duan, Dynamic fast flavor oscillation waves in dense neutrino gases, *Phys. Lett. B* **800**, 135088 (2020), [arXiv:1909.05225 \[hep-ph\]](#).
- [76] J. D. Martin, J. Carlson, V. Cirigliano, and H. Duan, Fast flavor oscillations in dense neutrino media with collisions, *Phys. Rev. D* **103**, 063001 (2021), [arXiv:2101.01278 \[hep-ph\]](#).
- [77] M. Zaizen and T. Morinaga, Nonlinear evolution of fast neutrino flavor conversion in the preshock region of core-collapse supernovae, *arXiv e-prints*, [arXiv:2104.10532](#) (2021), [arXiv:2104.10532 \[hep-ph\]](#).
- [78] Z. Xiong and Y.-Z. Qian, Stationary solutions for fast flavor oscillations of a homogeneous dense neutrino gas, *Phys. Lett. B* **820**, 136550 (2021), [arXiv:2104.05618 \[astro-ph.HE\]](#).
- [79] C. Kato, H. Nagakura, and T. Morinaga, Neutrino transport with Monte Carlo method: II. Quantum Kinetic Equations, *arXiv e-prints*, [arXiv:2108.06356](#) (2021), [arXiv:2108.06356 \[astro-ph.HE\]](#).
- [80] M.-R. Wu, M. George, C.-Y. Lin, and Z. Xiong, Collective fast neutrino flavor conversions in an 1D box: (I) initial condition and long-term evolution, *arXiv e-prints*, [arXiv:2108.09886](#) (2021), [arXiv:2108.09886 \[hep-ph\]](#).
- [81] S. Richers, D. E. Willcox, N. M. Ford, and A. Myers, Particle-in-cell Simulation of the Neutrino Fast Flavor Instability, *Phys. Rev. D* **103**, 083013 (2021), [arXiv:2101.02745 \[astro-ph.HE\]](#).
- [82] G. Sigl and G. Raffelt, General kinetic description of relativistic mixed neutrinos, *Nucl. Phys. B* **406**, 423 (1993).
- [83] S. Yamada, Boltzmann equations for neutrinos with flavor mixings, *Phys. Rev. D* **62**, 093026 (2000), [arXiv:astro-ph/0002502 \[astro-ph\]](#).
- [84] V. Cirigliano, C. Lee, M. J. Ramsey-Musolf, and S. Tulin, Flavored Quantum Boltzmann Equations, *Phys. Rev. D* **81**, 103503 (2010), [arXiv:0912.3523 \[hep-ph\]](#).
- [85] A. Vlasenko, G. M. Fuller, and V. Cirigliano, Neutrino Quantum Kinetics, *Phys. Rev. D* **89**, 105004 (2014), [arXiv:1309.2628 \[hep-ph\]](#).
- [86] D. N. Blaschke and V. Cirigliano, Neutrino Quantum Kinetic Equations: The Collision Term, *Phys. Rev. D* **94**, 033009 (2016), [arXiv:1605.09383 \[hep-ph\]](#).
- [87] H. Sasaki and T. Takiwaki, Neutrino-antineutrino oscillations induced by strong magnetic fields in dense matter, *Phys. Rev. D* **104**, 023018 (2021), [arXiv:2106.02181 \[hep-ph\]](#).
- [88] J. T. Pantaleone, Stability of incoherence in an isotropic gas of oscillating neutrinos, *Phys. Rev. D* **58**, 073002 (1998).
- [89] G. G. Raffelt and I. Tamborra, Synchronization versus decoherence of neutrino oscillations at intermediate densities, *Phys. Rev. D* **82**, 125004 (2010), [arXiv:1006.0002 \[hep-ph\]](#).
- [90] E. Akhmedov and A. Mirizzi, Another look at synchronized neutrino oscillations, *Nucl. Phys. B* **908**, 382 (2016), [arXiv:1601.07842 \[hep-ph\]](#).
- [91] Y. Kuramoto, *Chemical Oscillations, Waves, and Turbulence (Springer Series in Synergetics Book 19) (English Edition)*, kindle ed. (Springer, 2012) p. 158.